The Central Kiloparsec of Starbursts and AGN: The La Palma Connection
ASP Conference Series, Vol. 249, 2001
J. H. Knapen, J. E. Beckman, I. Shlosman, and T. J. Mahoney, eds.

Kinematics in the Central Kiloparsec of Spiral Galaxies

Johan H. Knapen

Isaac Newton Group of Telescopes, Apartado 321, E-38700 Santa Cruz de La Palma, Spain, and University of Hertfordshire, Department of Physical Sciences, Hatfield, Herts AL10 9AB, UK

Abstract. Results from kinematic observations of the central regions of spiral galaxies are reviewed, with particular emphasis on starburst and AGN hosts. While morphological studies lead to important insights, a more complete understanding of the physical processes that drive the evolution of the central regions can be achieved with measurements of the kinematics of gas and stars. Here, a variety of observational techniques at different wavelengths is critically discussed, and specific areas of interest are highlighted, such as inflow in barred galaxies and the origin of nuclear spiral arms. A brief discussion of a number of case studies is presented to illustrate recent progress.

1. Introduction

The study of the central regions of galaxies, and especially those hosting (circum)nuclear starbursts or AGN, which this conference is focused on, is of great importance for our understanding of a variety of astrophysical processes, ranging from those governing the existence and sustainment of the central activity, to the dynamics and evolution of galaxy disks. While progress on the observational front has been arguably lagging behind theory and modeling in the areas of, for example, bar dynamics and fueling of central activity, the availability of imaging at high angular resolution from the ground and from space has led to considerable progress on many morphological aspects (e.g., the review by van der Marel 2001; see also various papers in this volume). Tests of results and predictions from theory and modeling by fully sampled kinematic observations at similarly high resolution, however, are forthcoming only now. The fact that for many years after the pioneering papers on gas flows in bars (e.g., Sanders & Huntley 1976) the only two-dimensional kinematic mapping available was from H I studies, at angular resolutions of 15″ at best, illustrates this point. Only much later could gas kinematics be measured from molecular line observations, and even now CO interferometers are only just breaking the barrier of 1″ resolution (see §2.4).

This review is not meant to do justice to all those excellent papers on the topic which have appeared in the literature in recent years. Instead, an overview will be given of what can be learned from kinematic observations in a variety of objects, and what techniques can be used for which purpose. Recent progress is illustrated with a description of case studies of the core regions of two galaxies with circumnuclear ringlike structure, M100 and NGC 5248, for which kinematic observations lead to important tests and extensions of results

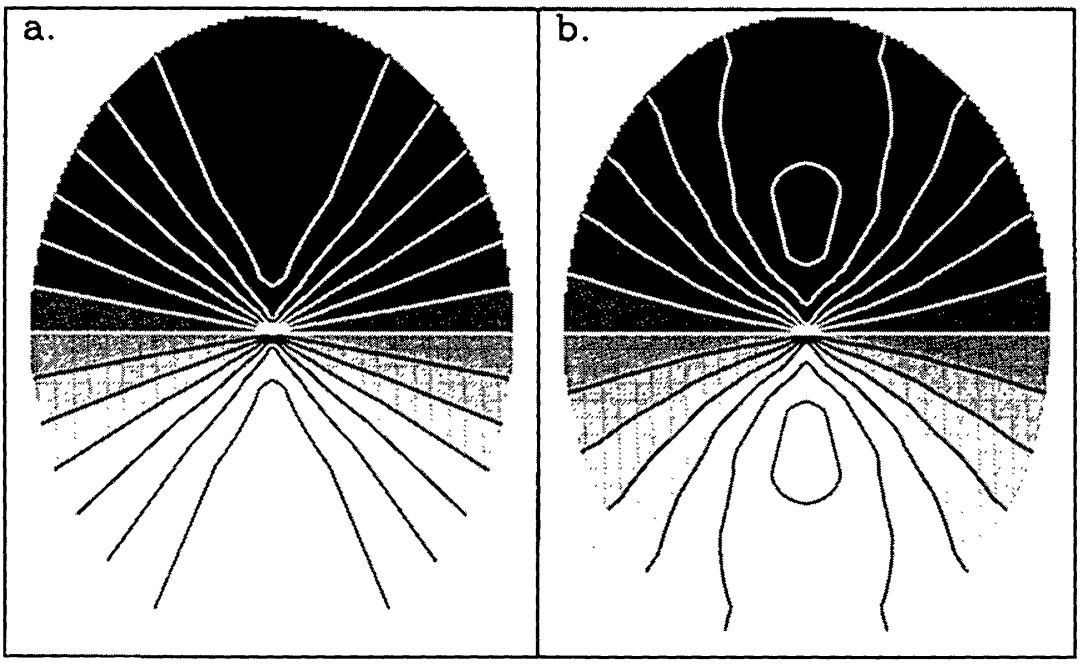

Figure 1. Examples of "spider diagrams": velocity fields produced from rapidly rising synthetic rotation curves, which *a)* reach a maximum and then remain flat (i.e., constant rotational velocity with increasing radius), and *b)* fall off after having reached a local maximum. Disk inclination is 45° in both cases.

obtained from imaging and modeling. Finally, some thoughts are given on the future of the field, which is very promising as new observatories and instruments come on line.

2. Observational Techniques

2.1. General Remarks

When making kinematic observations of galaxies, except possibly our own, one invariably measures blue- or redshifts of emission or absorption lines. One is also always limited to observing the line-of-sight velocity, or the component of the true velocity projected along the sight-line. A conventional way to display kinematic results is in the form of a velocity field, an image where (isovelocity) contours and/or color shades indicate the measured line-of-sight velocity. In the case of an inclined uniformly rotating disk, the velocity field takes the shape of a so-called "spider diagram", examples of which are shown in Figure 1. Velocity fields can be fitted to derive a rotation curve, which is the run of (deprojected) circular velocity with radius in a galaxy. Rotation curves often rise steeply in the central regions of galaxies. They flatten off close to the nucleus, sometimes after a few to tens of pc, although the measurement of this turnover depends critically on the spatial resolution of the observations. In many galaxies, rotation curves remain flat to radii well beyond the edge of the optical disk, which implies that

non-visible, dark matter is plentiful in the outer regions of those galaxies (see the review by Sofue & Rubin 2001 for an extensive discussion of rotation curves).

Gas and stars in a galaxy do not exclusively move on circular orbits, and deviations from disk rotation are seen in many velocity fields. The most important of such deviations are those caused by warps (not relevant for the present review), by bars and triaxial potentials, and by streaming across spiral arms (Figs. 3 and 4). Other effects, due to, for example, in- and outflows and shocks, are harder to recognize in velocity fields and can only be studied by analyzing and/or modeling the details of the full dataset or data cube (see, for example, the analysis of bar streaming presented in Knapen et al. 2000a). In many cases, a simple axisymmetric model velocity field produced from the rotation curve (Fig. 1) can be subtracted from the observed velocity field to highlight deviations from circular motion, such as those due to bars or spiral arms.

It is sometimes instructive to produce cuts through a kinematic dataset, and in fact this is often the only way to present subtle effects seen in the dataset. Such position–velocity (PV) diagrams can be made at random positions and position angles in the data cube, and thus mimic the result of optical/near-infrared (NIR) long-slit spectroscopy (see below).

2.2. Radio Wavelengths—The H I 21 cm Line

Because atomic hydrogen is rather optically thin, abundant in disk galaxies, and traces cold atomic gas, the H I 21 cm emission line is a near-perfect diagnostic for disks of galaxies. Unfortunately, however, H I in emission is generally not useful as a diagnostic in the central kpc regions of galaxies, because the low column density of the gas does not allow one to observe it at the required high spatial resolution.

The main use of H I in this area is its observation in absorption against a bright continuum source. Here, it is not the column density of the atomic hydrogen, but the brightness of the background continuum source that is the main limiting factor. This brightness may be so high as to allow the use of very long baseline interferometry (VLBI), and thus of very high spatial and spectral resolution observations of the cold gaseous component. This is nicely illustrated in recent work by Mundell et al. (2001), who observe H I at a spatial resolution of 25 mas or 1.6 pc in the nucleus of NGC 4151, and place constraints on the location of the AGN in the nuclear region. Morganti et al. (this volume, p. 632) give an overview of recent H I absorption results in a sample of radio galaxies, finding evidence for a wide range of phenomena related to the AGN, such as absorbing tori or outflows. Whereas the observation of H I absorption is obviously a very powerful technique, it is limited by the fact that not all galaxies have bright enough continuum emission to allow it to be used to its full extent. So although it can produce unique results at extremely high spatial and spectral resolution, this will only be the case for a limited numbers of galaxies which stand out by having strong nuclear radio-continuum emission.

2.3. Radio Wavelengths—Masers

Strong line emission by masers, mostly of the OH or H_2O molecules, also allows investigation of central kpc kinematics at extremely high resolution, using VLBI techniques. Maser emission traces high temperatures and gas densities, and often

traces rather extreme star formation (see theoretical reviews by Elitzur 2001 and Watson 2001 for more background).

As an example, we mention the MERLIN study of the 18 cm OH maser emission associated with the active (AGN and starburst) core of the ultraluminous infrared galaxy Markarian 273 by Yates et al. (2000). The brightest of three distinct regions of radio emission, two of which have clear NIR counterparts, harbors a 100 pc double-peaked structure, seen in NIR adaptive-optics and radio-continuum images (Knapen et al. 1997). The brightest component of the maser emission spatially resolved by Yates et al., shows ordered motion within the central 100 pc of the galaxy, which is aligned with the axis of the double-peaked structure, and which thus constrains the origin of this double peak. Other examples of the use of maser emission in the study of the central kpc of galaxies are given in the papers by Peck et al. and Pihlström, Conway & Booth (this volume, p. 321 and p. 646, respectively).

2.4. Millimeter Wavelengths—Molecular Lines

Molecular line transitions in the millimeter-wavelength domain, especially those of the CO molecule, have been used for many years as kinematic and morphological tracers of molecular gas in the central regions of galaxies (e.g., review by Combes 1999). CO emission is often directly interpreted as a measure of the mass of molecular hydrogen, through the use of a conversion factor, the so-called X-factor. This factor may well not be constant and its use in the central regions of galaxies with increased pressures, temperatures, radiation fields, and gas column densities may not be appropriate at all (e.g., Wall et al. 1993; Combes 1999; Regan 2000). Morphological information from CO observations is rather difficult to interpret, not only because hydrogen gas masses cannot be accurately estimated, but also because local processes, e.g., star formation, may change the X-factor within a small area.

Millimeter interferometers, such as ATCA, BIMA, IRAM, NRO, or OVRO, now routinely deliver observations at millimeter wavelengths at spatial resolutions of around or below one arcsecond. Many examples of such observations were presented at this conference (papers in Part 7 of this volume). The datasets contain information on kinematics as well as morphology. Here, the X-factor is generally less of a problem, because even if the CO emission at a certain point does not quite trace the mass of molecular hydrogen, it will most probably still trace the same line-of-sight velocity, namely that of the molecular cloud of which both CO and H_2 are part. The kinematics of cold molecular gas, a dissipative collisional component, constitute a sensitive tracer of the stellar potential. Upcoming developments over the next few years include the Combined Array for Research in Millimeter Astronomy (CARMA) which will combine the OVRO amd BIMA antennas at a new high-altitude site to provide a heterogeneous mm-wave array with highly improved sensitivity, imaging speed, and fidelity, and the Atacama Large Millimeter Array (ALMA) project, which is now well under way.

2.5. Optical/NIR: Long-Slit Spectroscopy

The technique of long-slit spectroscopy is often used for kinematic measurements to derive line-of-sight velocities and velocity dispersions along certain position

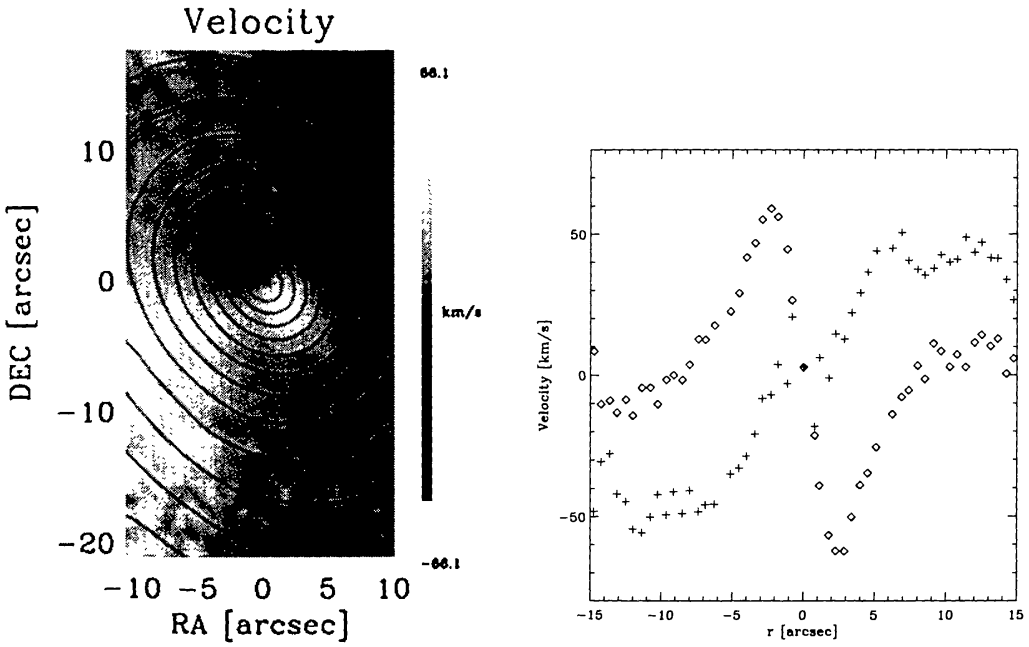

Figure 2. *Left:* Velocity field of the central region of NGC 4365 (*grays*), and total-intensity map (*contours*). The velocities were measured using the spectral region around the Mg *b* feature at $\sim$ 5180 Å. *Right:* Extractions from the Sauron data cube along the major (*open diamonds*) and minor (*plus signs*) axes. (*Based upon SAURON data from Davies et al. 2001.*)

angles in extended objects. Applications include the determination of central mass concentrations and masses of massive black holes (MBHs), and the overall kinematics of bars.

Although long-slit spectroscopy can be used to measure the kinematic structure of the central kpc regions of galaxies, two-dimensional velocity maps allow the precise location of different kinematic components. This is nicely illustrated by the case of the central region of the galaxy NGC 4365, of which Davies et al. (2001) publish the velocity field as observed with the SAURON instrument (Bacon et al. 2001a; see also §2.7) on the William Herschel Telescope (WHT). Surma & Bender (1995) obtained long-slit spectra of this same galaxy and interpreted the kinematic behavior as evidence for a decoupled core. The velocity field of Davies et al., confirms this result, but also shows in detail how the line of nodes of the velocity field rotates by $\sim$ 100 degrees in the core region of the galaxy. Moreover, the information on line strengths extracted from their observations allows Davies et al., to conclude that the two kinematically distinct components have a common age and star formation history. In Fig. 2, the SAURON velocity field of the inner region of NGC 4365 is shown in grayscales, with contours indicating the intensity as reconstructed from the SAURON data (left panel). The right panel shows two synthetic "long-slit spectra", extractions from the SAURON data cube along the major axis (open diamonds) and along the minor axis (plus signs). The difference between these is striking but its origin can be easily understood from the velocity field.

2.6. Optical/NIR: Fabry–Pérot

The way forward in the kinematic study of the central regions of galaxies is by mapping the two-dimensional velocity structure, or three-dimensional imaging as this is sometimes referred to (where the third dimension is velocity, the third axis in cubes of images). Radio interferometry gives this kind of imaging, but there are also several ways to achieve this in the optical-NIR. One of these is by the use of Fabry–Pérot interferometers, which, after data reduction, produce a set of fully sampled images, each at a slightly different wavelength or velocity. These datasets or data cubes can then be treated in several ways, but much in the same way as radio interferometry datasets are analyzed, e.g., through Gaussian or moment fitting of the individual spectral profiles.

The advantage of Fabry–Pérot interferometers is that they deliver fully sampled high spatial resolution kinematic datasets over decent fields (few arcmin at subarcsec resolution). Data reduction used to be cumbersome but is no longer a serious problem with modern computers and data analysis software. A disadvantage of this technique is that it is rather expensive of observing time because only a very small wavelength range can be scanned during one observation (almost always one spectral line only). Fabry–Pérot interferometers remain powerful for kinematic studies of galaxy disks and the central regions thereof (Figs. 3 and 4), but for small fields of view in central kpc regions integral-field spectrographs (IFSs) are very competitive, as described briefly in the following section.

2.7. Optical/NIR: Integral-Field Spectrographs

IFSs are becoming more and more popular, and nowadays form part of the standard instrumentation suite of most major telescopes, including those in the 8 m class. The basic idea is to divide the incoming focal-plane image into a number of small independent sub-images, sometimes referred to as micropupils. These are dispersed and form individual spectra, which are subsequently captured on a CCD or NIR array detector. Spectra are thus obtained simultaneously for a range of (x, y) positions across the image. In the data reduction stage, the individual spectra can be combined into maps of the source by extracting specific parameters, such as velocity, line strength, or velocity dispersion, of a certain spectral line. In one observation, one can thus obtain maps of all these quantities, built up of a number of independent "pixels" which equals the number of individual micropupils into which the original focal-plane image of the source was divided. This basic idea is common to all IFSs, although in practice several techniques are in use to divide the focal-plane image, namely by employing a lenslet array (e.g., SAURON, Bacon et al. 2001a; Krajnovic, this volume, p. 699), a fiber bundle (e.g., INTEGRAL, Arribas et al. 1998; García-Lorenzo, this volume, p. 175), or an image slicer (e.g. the IFS in GNIRS for Gemini, Dubbeldam et al. 2000).

Integral-field spectrographs are becoming increasingly more powerful because 1) more and more fibers/lenslets can be used, due in turn to technical improvements in the fibers/lenslets themselves and to larger CCDs; 2) fibers can be more closely packed, thus allowing better sampling; 3) IFSs are now beginning to be implemented on 8 m class telescopes; and 4) IFSs will be cou-

pled to adaptive-optics units, thus allowing for spectral imaging at much higher spatial resolutions (e.g., Bacon et al. 2001b).

3. Kinematic Information on Starbursts and AGN

Kinematic observations can reveal important clues on dynamical processes related to the overall behavior of the host galaxy, to the fueling of the central regions by gas from the disk, and/or to dynamical feedback, where material is expelled by the AGN or by massive newly formed stars. Some of the most important of these processes are outlined in this section for objects with different classes of activity in the central kpc.

3.1. Bulges and Black Holes

The dynamical study of bulges in general is outside the scope of this review, but the relationships between the properties of bulges and those of the MBHs they may harbor is of interest here. Full details of the progress in this area can be found in the comprehensive review by Merritt & Ferrarese (this volume, p. 335). Kinematic measurements are used to estimate the amount of enclosed mass, in turn leading to a determination of MBH mass, and to study the dynamics of bulges. Although other techniques are used (e.g., imaging and modeling of central cusps in the light distribution, e.g., van der Marel 1999; so-called reverberation mapping of the broad emission line region of AGN, e.g., Peterson 1993; or direct measurement of proper motions of individual stars near the nucleus of our Milky Way, e.g., Genzel et al. 2000), spectroscopy is the most widely used tool to determine enclosed masses, by measuring the circular rotation velocity at small radii and deriving the enclosed mass needed to maintain this rotation (e.g., Miyoshi et al. 1995; Salucci et al. 2000; Hughes et al., this volume, p. 363). In order to constrain the MBH mass, the rotation measurement must be made as far inside the bulge of the galaxy as possible, hence the need for high spatial resolution spectroscopy, e.g., with VLBI or the *HST*.

Kinematic measurements of observable properties of bulges, such as their velocity dispersion, have recently led to a number of most interesting correlations between such properties and MBH masses, as described in detail by Merritt & Ferrarese (this volume, p. 335).

3.2. AGN and Their Hosts

Kinematic observations of AGN and their host galaxies are used to investigate important problems, such as how AGN are fueled by gaseous material from the disk, or how the energy released by an AGN influences its surroundings (the first of these is relevant to all kinds of central activity, not just non-stellar).

Already for two decades, a number of authors have argued on the basis of theory and modeling that bars, or sets of nested bars, can transport gaseous material from the disks of galaxies toward their central regions, basically because part of the angular momentum of the gas is dissipated by the bars (e.g., Schwarz 1981; Combes & Gerin 1985; Shlosman, Frank, & Begelman 1989; Friedli & Benz 1993). This idea is hard to confirm kinematically because 1) not all the inflowing gas may reach the central region of the galaxy (e.g., Knapen et al. 1995a; Regan,

Vogel, & Teuben 1997); 2) observationally, one is always restricted to measuring the line-of-sight velocities and biased to observing those around the minor axis; and 3) the gas masses needed to fuel and sustain even the most powerful AGN or starburst are relatively small, of the order of a few solar masses per year, and may be brought about by inflow speeds that are so low that they are hard to measure (Kenney 1994). As a result, only few authors have published inflow rates, calculated indirectly by estimating the gravitational torque exerted on the gas by the stellar bar potential (Quillen et al. 1995), or by comparison with hydrodynamical models (Regan et al. 1997). Net inflow velocities of 10–20 km s^{-1} were found, with net gas inflow of order one to a few solar masses per year. Wong & Blitz (2000) find some evidence for inflow from an analysis of H I data of NGC 4736, but warn that their inferred inflow velocities are too high and would need further analysis. Even when considering these few determinations of inflow velocities, it must be kept in mind that in all cases the line-of-sight velocity observations are compared to a dynamical model, which implies a number of assumptions on, for example, the mass-to-light ratio or the pattern speed. We conclude that although the overall case for gas inflow regulated by galactic bars is strong, it remains difficult to find direct evidence for the inflow.

3.3. Starburst Galaxies

A causal link has long since been established between the presence of central starbursts and bars in galaxies (e.g., Heckman 1980; Balzano 1983; Hawarden et al. 1986; Devereux 1987; Puxley, Hawarden, & Mountain 1988; Kennicutt 1994), which, when combined with our knowledge of bars from theory and modeling, makes for compelling evidence that bars fuel the starbursts by channeling disk material inwards. This is different from the situation in AGN hosts, where only recently evidence has been found for a slight excess of bars in Seyferts when compared to non-Seyfert galaxies (see Knapen, Shlosman, & Peletier 2000b; Laine et al. 2001a; also Laine et al., this volume, p. 112). As discussed above, though, the kinematics of this bar-driven inflow of gas remain difficult to observe directly.

Massive stars in starbursts deposit energy in the surrounding interstellar medium through supernovae and stellar winds, which give rise to outflows of gas on galactic scales, so-called superwinds (see Heckman 2001 for a recent review). Superwinds are ubiquitous in the most actively star-forming galaxies, both locally (e.g., Lehnert & Heckman 1996) and at high redshift (Pettini et al. 2001). Depending on the amount of energy and duration of the wind, and on the properties of the halo, the superwind may break out of the disk of its host galaxy and form a weakly collimated bipolar outflow cone at scales of tens of kiloparsec, roughly perpendicular to the disk. X-ray emission is observed from the hot material in the superwind (e.g., Strickland et al. 2000). Multi-wavelength observations of the cold, warm, and hot phases of the interstellar medium (ISM) associated with the starburst-driven outflow can yield information on the energetics, dynamics, and propagation of the starburst, while the dynamical timescale as determined from the size and kinematics of the outflow can constrain the starburst age (e.g., Elmegreen 1992; Elmegreen & Lada 1977; Jogee, Kenney, & Smith 1998; Calzetti et al. 1999; Chapman et al. 2000a).

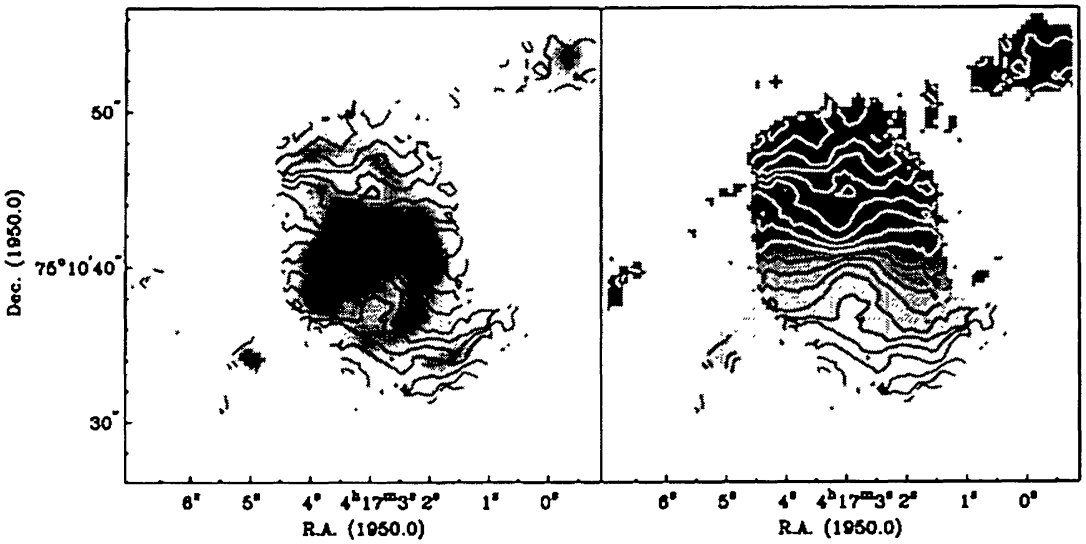

Figure 3. Hα Fabry–Pérot total-intensity map (*left*, in *greys*) and velocity field (*right*, in *greys*; in both *panels* in *contours*) of the central region of NGC 1530, as obtained with the 4.2 m WHT on La Palma. The spatial resolution is $\sim 0\farcs9$.

3.4. Circumnuclear Star-Forming Regions

Nuclear rings are rather common in barred galaxies (although precise statistics are still missing), and are believed to occur where inflowing gas slows down near the location of one or more inner Lindblad resonances (ILRs; see review by Shlosman 1999; §4). Kinematic observations can be used in this respect to study the gas motions in the bar, which give information on the bar dynamics and possibly the inflow velocities and masses (see above). To a first approximation, and in the case of very weak bars *only*, rotation curves can be used to estimate where the ILRs are expected to lie (basically near the turnover in the rotation curve).

Velocity fields of the circumnuclear regions usually show predominantly circular rotation, but often also non-circular motions caused by deviations from axisymmetry. The latter give detailed kinematic information on spiral arms or inner bars that can be used to test and constrain dynamical modeling (e.g. Knapen et al. 2000a; §4). As an illustration, we show here TAURUS Fabry–Pérot results on the core region of NGC 1530 (Fig. 3), where the rotation is revealed as a spider diagram outlined by the isovelocity contours in the velocity field. The wiggles and curves in the contours are due to gas streaming around the bar, and to spiral density wave streaming in the nuclear star-forming region (Relaño et al., in preparation).

4. Central kpc Kinematics in M100

M100 (= NGC 4321) has a bar of moderate strength which gives rise to a particularly clear resonant circumnuclear structure (Knapen et al. 1995a). It is a prime example of a class of barred galaxies which host circumnuclear ringlike

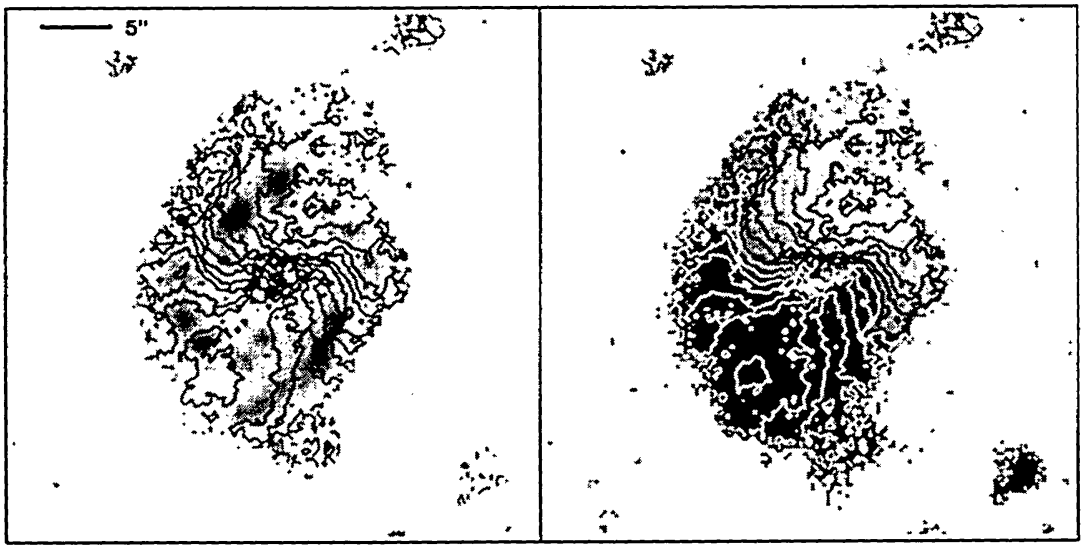

Figure 4. Hα FP moment maps of the central region of M100: the velocity field is shown in *contours* and overlaid on the total-intensity Hα image (*left*), and on the velocity field itself (*right*). *Contours* are separated by 15 km s^{-1}, from 1480 km s^{-1} to 1675 km s^{-1}. *Black contours* in the *right panel* are low velocities; the first *white contour* is at 1585 km s^{-1}. N is *up*, E to the *left*.

star-forming or starburst activity (see review on rings by Buta & Combes 1996). In the NIR, the morphology of the core is that of an annular star-forming zone surrounding a small, nuclear, stellar bar. In the optical, and especially in star formation tracers such as Hα, individual star-forming sites are clearly recognized within the ringlike region and are spread along miniature spiral armlets. The dust lane morphology shows that these spiral arms form a twofold symmetrical, or grand-design, pattern, which connects through the bar and out into the disk of the galaxy (Knapen et al. 1995a,b). We modeled these and other observed features in M100 numerically in terms of a resonant structure driven by one bar. The bar is dissected by the ringlike star-forming region, located between a pair of ILRs. Although the hydrodynamical modeling and interpretation agreed in great detail to the morphology as determined from a variety of images, we decided to test the model results directly with kinematic measurements.

We used the TAURUS II instrument in Fabry–Pérot mode on the WHT on La Palma to make two-dimensional kinematic observations in the Hα line of the circumnuclear region of M100. The $\sim$ 0.″7 seeing was well sampled with 0.″28 pixels. After wavelength and phase calibration we produced a cube containing a series of spatial maps at increasing wavelength, and thus velocity (Knapen et al. 2000a).

After determining which channels of the dataset were free of Hα line emission, we used those channels to determine and subtract the continuum emission. A moment analysis was used to produce a total intensity map (moment zero) and a velocity field (moment one) in Hα; these are shown in Figure 4. Proof of the reliability of the FP technique is the fact that the total intensity Hα map, thus reconstructed, is comparable in quality to the narrow-band Hα image published

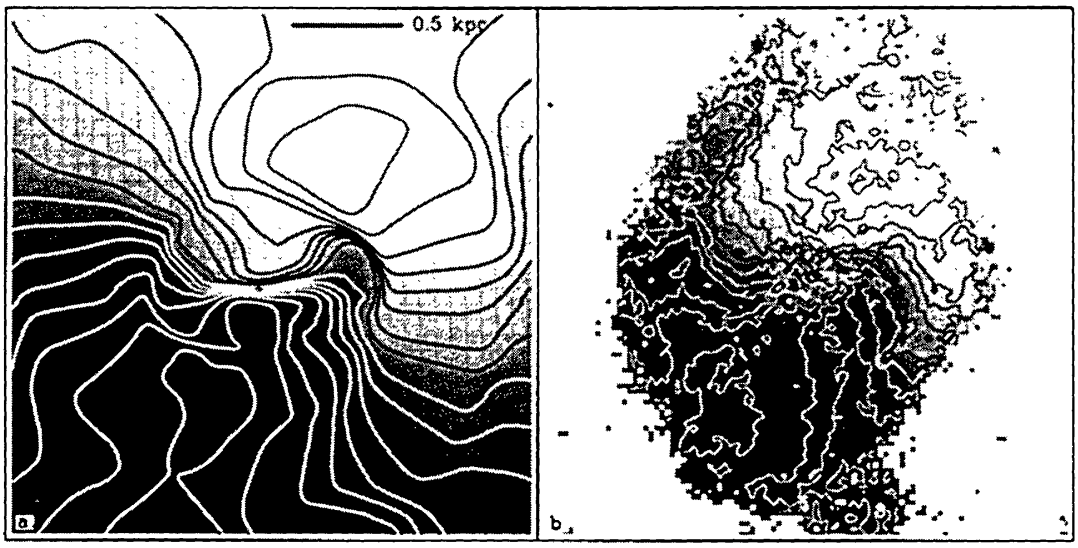

Figure 5. *Left panel:* Gas velocity field as derived from the numerical model of Knapen et al. (1995a). *Contour* separation is 15 km s^{-1}, and the scale is indicated in the *top right-hand corner*. N is *up*, E to the *right*. The position angle of the major axis is as in M100. Resolution is comparable to our Hα data. *Right panel:* For comparison, Hα velocity field of Fig. 3 at the same scale and orientation, and with the same *contour* separation. (*From Knapen et al. 2000a.*)

by Knapen et al. (1995b), with an estimated spatial resolution of 0.″6–0.″7. Although the velocity field is dominated by circular motions, and a rotation curve can be derived, it does show important deviations from circular motion. The positions where these deviations take place can be related to the total-intensity map. A more detailed analysis of the data cube confirms that the deviations are due to streaming motions in the spiral arms, and to a lesser extent, to gas streaming along the inner part of the bar (see Knapen et al. 2000a for more details). We thus showed kinematically that the spiral armlets are density-wave spiral arms, and that the elongation in the NIR isophotes is in fact due to a bar, as reported before (Knapen et al. 1995a,b).

To make a detailed kinematic comparison with the new Hα FP data, we produced a velocity field from our SPH dynamical model of the CNR of M100 (Knapen et al. 1995a), which was made before the kinematic data became available. The result of that comparison is shown in Figure 5. The qualitative and quantitative agreement between the model and Hα velocity fields, as outlined in this figure, gives further support to our interpretation of the CNR in terms of a resonance region driven by one bar, dissected by the ringlike region which hosts the star-forming spiral armlets.

5. The Core of NGC 5248

Nuclear spirals have recently been discovered in a considerable number of spiral galaxies of varying types, thanks exclusively to the availability of high-resolution imaging, especially in the NIR, both from space using the *HST* and from the

ground using adaptive optics (e.g., Ford et al. 1994; Phillips et al. 1996; Grillmair et al. 1997; Devereux, Ford, & Jacoby 1997; Dopita et al. 1997; Carollo, Stiavelli, & Mack 1998; Elmegreen et al. 1998; Malkan, Gorjian, & Tam 1998; Rouan et al. 1998; Laine et al. 1999; Martini & Pogge 1999; Regan & Mulchaey 1999; Chapman, Morris, & Walker 2000b; Tran et al. 2001). This nuclear spiral structure, most often seen in dust, occurs at scales of a few tens to hundreds of parsec, and is in the great majority of cases flocculent in appearance. In a handful of galaxies, however, nuclear grand-design spirals are found (NGC 5248 in Laine et al. 1999; UGC 12138 and NGC 7682 in Martini & Pogge 1999). The importance of nuclear spirals lies in a number of key areas like the nature of spiral structure, its behavior in the presence of dynamical resonances, or the possible role of spirals in fueling nuclear activity.

There are three main theoretical schemes to explain the existence of nuclear spiral arms within the location of the ILR(s). It is relatively easy to distinguish between these schemes with suitable observations, *if* the right observations at sufficiently high spatial resolution are available. First, a nuclear spiral pattern can exist within the inner ILR of the outer spiral pattern. The nuclear spiral must in this case have a much higher pattern speed than the dynamically independent large spiral pattern in the disk (Heller & Shlosman 1994; Englmaier & Shlosman 2000). Second, as described and modeled by Englmaier & Shlosman (2000), the large-scale bar or outer spiral pattern can drive the nuclear spiral, and the pattern speeds of both sets of spirals must be equal. The potential well must in this case be shallow enough to prevent the spiral from winding up and destroying itself by dissipation. A third possibility is that nuclear spiral arms, but exclusively flocculent ones, are formed by acoustic instabilities, as described by Elmegreen et al. (1998; see also Montenegro, Yuan, & Elmegreen 1999).

A good illustration of the power of a complete kinematic analysis of the central regions of galaxies is given by the case study of the nuclear spiral arms in the core of NGC 5248, which is in fact the first kinematic study of nuclear spirals. The spiral structure in NGC 5248 can be identified as very faint outer stellar arms, at scales of tens of kpc, classical optically bright star formation arms at scales of a few kpc, gas/dust arms at the inner ends of the star formation spirals, and the grand-design nuclear spiral at scales of tens to a few hundreds of pc, reported by Laine et al. (1999) on the basis of adaptive-optics NIR imaging. NGC 5248 hosts a circumnuclear star-forming ring, containing a number of UV-bright knots of star formation (see Maoz et al. 2001). In addition to this ring with a diameter of some 14 arcsec (1.1 kpc), there is another pseudo-ring, visible in Hα, which encircles the nucleus at a radius of 1 arcsec. This innermost ring thus lies in the same region as the grand-design nuclear spirals, but its relation to those spirals, or in fact its origin, is not known (Laine et al. 2001b; Maoz et al. 2001).

Laine et al. (1999) suggested that the nuclear spiral may have formed through the second of the three mechanisms described above, i.e., it is dynamically coupled to the outer spiral. In order to test this hypothesis, we obtained a fully sampled two-dimensional set of kinematic data using TAURUS on the WHT. The resulting dataset has a spatial resolution of around 0.9 arcsec (68 pc) and a spectral resolution corresponding to 18.9 km s^{-1} (see Laine et al. 2001b for details). The morphology is dominated by the nuclear ring with its strong star

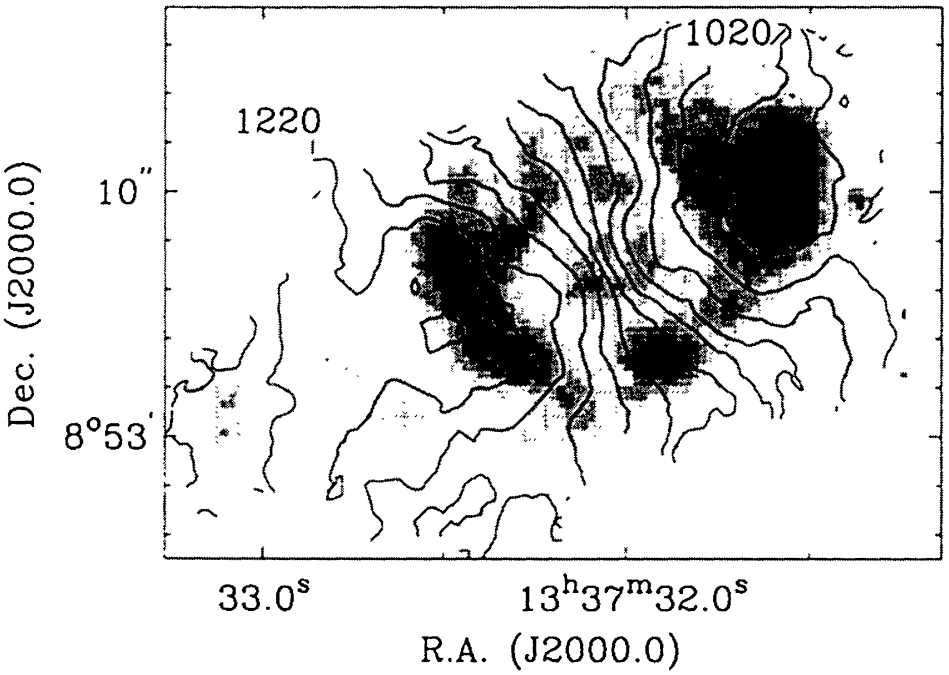

Figure 6. Hα Fabry–Pérot total-intensity map and velocity field of the central region of NGC 5248, as obtained with the WHT. Spatial resolution ~ 0.″8, and selected *contours* are labeled with velocity in km s^{-1}. (*Reproduced with permission from Laine et al. 2001b.*)

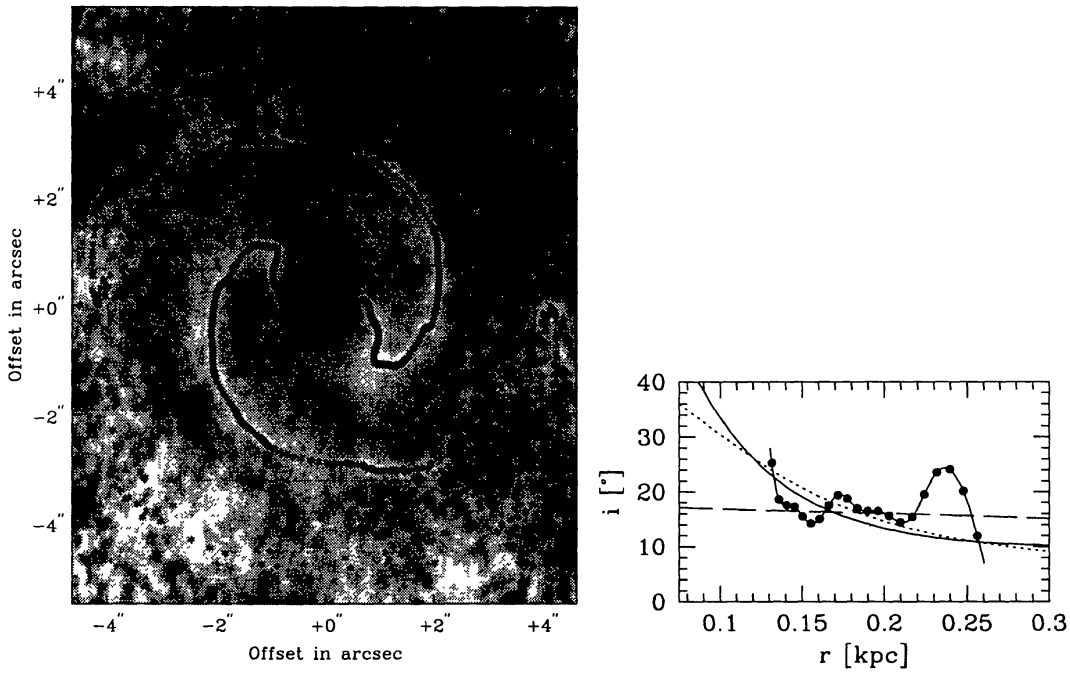

Figure 7. Fitted nuclear spirals from AO $J-K$ image (*left*), and the observed pitch angle compared to models (*right*). (*Reproduced with permission from Laine et al. 2001b.*)

formation knots, but also the innermost pseudo-ring is visible. The kinematic structure is dominated by circular rotation, where the closed contours on both sides of the nucleus imply that the rotation is falling after reaching a local maximum (Fig. 6). In marked contrast to the circumnuclear region in M100 (see above), which is morphologically similar, non-circular motions are practically absent from the velocity field of the core of NGC 5248—from the circumnuclear as well as from the nuclear spiral region. The well-resolved rotation curve as derived from the velocity field (Fig. 6) shows a relatively shallow rise in the curve (in contrast to, for example, M100 [Knapen et al. 2000a]; or many other spiral galaxies [Sofue & Rubin 2001]).

In order to consider the main parameter determining the nature of the nuclear spiral pattern, namely its pattern speed in comparison with that of the main spiral pattern, a combination of morphology, kinematics and modeling is needed. Laine et al. (2001b) measured the pitch angle of the nuclear spiral arm in the $J-K$ adaptive-optics image from Laine et al. (1999). They also derived the rotation curve from the kinematic velocity field in the same radial range ($1\farcs8$ – $3\farcs4$). Using analytical modeling based upon Englmaier & Shlosman (2000) and the rotation curve, the pitch angle of the nuclear spiral was subsequently modeled (Fig. 7). From this comparison Laine et al., concluded that the observed (from the $J-K$ adaptive-optics image) and modeled (from the rotation curve) pitch angles agree well for a low pattern speed ($\Omega_{\rm P} = 13$ km s^{-1} kpc^{-1}) and "normal" ISM sound speed ($c_{\rm s} = 9-16$ km s^{-1}). This is the pattern speed derived by Patsis, Grosbøl, & Hiotelis (1997) for the outer spiral, and the best agreement in the modeling is thus found by using equal, low pattern speeds for the outer and nuclear spirals. High pattern speed values for the nuclear spiral are specifically excluded because they are incompatible with the observed arm pitch angle. The acoustic spiral theory of Elmegreen et al. (1998) is not applicable in this case of a grand-design two-armed spiral, because that mechanism will produce chaotic and multi-armed spirals.

The conclusion from the kinematic observations of Laine et al. (2001b), after combining them with high-resolution imaging and modeling, is thus that the nuclear spiral rotates at the same rate as the outer spiral (the second of the three theoretical scenarios outlined above). This implies that the spiral structure is dynamically coupled from scales of a few tens of pc to several kpc. Transport and distribution of gas from the disk to the core region, over orders of magnitude in scale, is controlled by coupled mechanisms.

6. Final Remarks and Future Prospects

A considerable variety of techniques is used to study the kinematics of gas and stars at different wavelengths, and on different spatial scales, in the central regions of galaxies. I have reviewed some of these and indicated how they can increase our understanding of various aspects of galaxies and especially those hosting (circum)nuclear starbursts and AGN. Although all of the techniques mentioned will remain in use in the future, some have particular promise. First, integral-field spectrographs will become more powerful a) when more and more image elements can be fed to spectrographs and onto ever larger detectors, thus increasing the spatial resolution, sampling, and/or the field of view, b) when used

on 8 m class telescopes, and c) when used in conjunction with AO units. Secondly, upgrades to existing millimeter interferometers will continue to increase the spatial resolution and sensitivity of kinematic data obtained, mostly in the CO lines. ALMA is expected to revolutionize this field also when it becomes operational, sometime later this decade, allowing observations at spectacularly improved sensitivities and spatial resolutions of the central kpc regions of galaxies with a wide variety of central activity. Observations with such improved or new facilities, along with continued progress in modeling and theory, will no doubt lead to fascinating new insights into the how, why, and when of central activity in galaxies.

In a number of examples we have shown that there is firm evidence that the central kpc regions of galaxies are firmly embedded in, and dynamically directly coupled to, the spiral arms in the main disk of the galaxy. In M100, a combination of extensive imaging and kinematic observations at various wavelengths with detailed numerical modeling has shown that the circumnuclear structure in this galaxy is resonant in origin, and is being maintained and fed by a bar structure. Within the ringlike region of enhanced star formation and gas density, which is related to the position of a pair of ILRs, density-wave spiral arms occur, directly coupled dynamically to the spiral arms in the main disk of the galaxy. In NGC 5248, the dynamical coupling of spiral arm systems is occurring over an even larger range of length scales. Kinematic observations in conjunction with analytic and numerical modeling and adaptive-optics imaging shows that the nuclear grand-design spiral at scales of tens of pc rotates with equal pattern speed to the outer spiral, on scales of a few kpc.

Acknowledgments. I thank my collaborators on the various projects mentioned in this paper, especially Seppo Laine, Isaac Shlosman, Reynier Peletier, and Shardha Jogee. I thank Harald Kuntschner and the SAURON team for their help in preparing Figure 2. The William Herschel Telescope is operated on the island of La Palma by the Isaac Newton Group in the Spanish Observatorio del Roque de los Muchachos of the Instituto de Astrofísica de Canarias.

References

Arribas, S., et al., 1998, Proc. SPIE, 3355, 821

Bacon, R. et al. 2001a, MNRAS, 326, 23

Bacon, R., Emsellem, E., Combes, F., Copin, Y., Monnet, G., & Martin, P., 2001b, A&A, 371, 409

Balzano, V. A. 1983, ApJ, 268, 602

Buta R., & Combes F. 1996, Fund. Cosmic Phys., 17, 95

Calzetti, D., Conselice, C. J., Gallagher, J. S.. & Kinney, A. L. 1999, AJ, 118, 797

Carollo, C. M., Stiavelli, M.. & Mack, J. 1998, AJ, 116, 68

Chapman, S. C., Morris, S. L., Alonso-Herrero, A.. & Falcke, H. 2000a, MNRAS, 314, 263

Chapman, S. C., Morris, S. L.. & Walker, G. A. H. 2000b, MNRAS, 319, 666

Combes, F.. & Gerin, M. 1985, A&A, 150, 327

Combes, F. 1999, in ASP Conf. Ser., vol. 187, The Evolution of Galaxies on Cosmological Timescales, ed. J. E. Beckman & T. J. Mahoney (San Francisco: ASP), p. 59

Davies, R. L., et al. 2001, ApJ, 548, L33

Devereux, N. A. 1987, ApJ, 323, 91

Devereux, N., Ford, H., & Jacoby, G. 1997, ApJ, 481, L71

Dopita, M.,A., Koratkar, A. P., Allen, M. G., Tsvetanov, Z. I., Ford, H. C., Bicknell, G. V., & Sutherland, R. S. 1997, ApJ, 490, 202

Dubbeldam, M., Content, R., Allington-Smith, J. R., Pokrovski, S., & Robertson, D. J. 2000, Proc. SPIE, 4008, 1181

Elitzur, M. 2001, in IAU Symp. 206, Cosmic Masers, ed. V. Migenes & E. Luedke (San Francisco: ASP), in press (astro-ph/0105205)

Elmegreen, B. G. 1992, in Star Formation in Stellar Systems, eds. G. Tenorio-Tagle, M. Prieto, & F. Sánchez, (Cambridge: Cambridge University Press), p. 381

Elmegreen, B. G., & Lada, C. J. 1977, ApJ, 214, 725

Elmegreen, B. G., et al. 1998, ApJ, 503, L119

Englmaier, P., & Shlosman, I. 2000, ApJ, 528, 677

Ford, H. C., et al. 1994, ApJ, 435, L27

Friedli, D., & Benz, W. 1993, A&A, 268, 65

Genzel, R., Pichon, C., Eckart, A., Gerhard, O. E., & Ott, T. 2000, MNRAS, 317, 348

Grillmair, C. J., Faber, S. M., Lauer, T. R., Hester, J. J., Lynds, C. R., O'Neil, E. J., Jr., & Scowen, P. A. 1997, AJ, 113, 225

Hawarden, T. G., Mountain, C. M., Leggett, S. K., & Puxley, P. J. 1986, MNRAS, 221, 41P

Heckman, T. 1980, A&A 88, 365

Heckman, T. 2001, in ASP Conf. Ser., Extragalactic Gas at Low Redshift, ed. J. Mulchaey & J. Stocke (San Francisco: ASP), in press (astro-ph/0107438)

Heller, C. H., & Shlosman, I. 1994, ApJ, 424, 84

Jogee, S., Kenney, J. D. P., & Smith, B. J. 1998, ApJ, 494, L185

Kenney, J. D. P. 1994, in Mass-Transfer Induced Activity in Galaxies, ed. I. Shlosman (Cambridge: Cambridge University Press), p. 78

Kennicutt, R. C. 1994, in Mass-Transfer Induced Activity in Galaxies, ed. I. Shlosman (Cambridge: Cambridge University Press), p. 131

Knapen, J. H., Beckman, J. E., Heller, C. H., Shlosman, I., & de Jong, R. S. 1995a, ApJ, 454, 623

Knapen, J. H., Beckman, J. E., Shlosman, I., Peletier, R. F., Heller, C. H., & de Jong, R. S. 1995b, ApJ, 443, L73

Knapen, J. H., Laine, S., Yates, J. A., Robinson, A., Richards, A. M. S., Doyon, R., & Nadeau, D. 1997, ApJ, 490, L29

Knapen, J. H., Shlosman, I., Heller, C. H., Rand, R. J., Beckman, J. E., & Rozas, M. 2000a, ApJ, 528, 219

Knapen, J. H., Shlosman, I., & Peletier, R. F. 2000b, ApJ, 529, 93

Laine, S., Knapen, J. H., Pérez-Ramírez, D., Doyon, R., & Nadeau, D. 1999, MNRAS, 302, L33

Laine, S., Knapen, J. H., Pérez-Ramírez, D., Englmaier, P., & Matthias, M. 2001b, MNRAS, 324, 891

Laine, S., Shlosman, I., Knapen, J.H., & Peletier, R. F. 2001a, ApJ, in press (astro-ph/0108029)

Lehnert, M. D., & Heckman, T. M. 1996, ApJ, 462, 651

Malkan, M., Gorjian, V., & Tam, R. 1998, ApJS, 117, 25

Maoz, D., Barth, A. J., Ho, L. C., Sternberg, A., & Filippenko, A. V. 2001, AJ, 121, 3048

Martini, P., & Pogge, R. W. 1999, AJ, 118, 2646

Miyoshi, M., Moran, J., Herrnstein, J., Greenhill, L., Nakai, N., Diamond, P., & Inoue, M. 1995, Nat, 373, 127

Montenegro, L. E., Yuan, C., & Elmegreen, B. G. 1999, ApJ, 520, 592

Mundell, C. G., Wrobel, J. M., Pedlar, A., & Gallimore, J. F. 2001, in IAU Symp. 205, Galaxies and Their Constituents at the Highest Angular Resolutions, ed. R. Schilizzi, S. Vogel, F. Paresce, & M. Elvis (San Francisco: ASP), in press (astro-ph/0012229)

Patsis, P., Grosbøl, P., & Hiotelis, N. 1997, A&A, 323, 762

Peterson, B. M. 1993, PASP, 105, 247

Pettini, M., Shapley, A. E., Steidel, C. C., Cuby, J., Dickinson, M., Moorwood, A. F. M., Adelberger, K. L., & Giavalisco, M. 2001, ApJ, 554, 981

Phillips, A. C., Illingworth, G. D., MacKenty, J. W., & Franx, M. 1996, AJ, 111, 1566

Puxley, P. J., Hawarden, T. G., & Mountain, C. M. 1988, MNRAS, 231, 465

Quillen, A. C., Frogel, J. A., Kenney, J. D. P., Pogge, R. W., & Depoy, D. L. 1995, ApJ, 441, 549

Regan, M. W. 2000, ApJ, 541, 142

Regan, M. W., Vogel, S. N., & Teuben P. J. 1997, ApJ, 482, L143

Regan, M. W., & Mulchaey, J. S. 1999, AJ, 117, 2676

Rouan, D., Rigaut, F., Alloin, D., Doyon, R., Lai, O., Crampton, D., Gendron, E., & Arsenault, R. 1998, A&A, 339, 687

Salucci, P., Ratnam, C., Monaco, P., & Danese, L. 2000, MNRAS, 317, 488

Sanders, R. H., & Huntley, J. M. 1976, ApJ, 209, 53

Schwarz, M. P. 1981, ApJ, 247, 77

Shlosman, I. 1999, in ASP Conf. Ser., vol. 187, The Evolution of Galaxies on Cosmological Timescales, ed. J. E. Beckman & T. J. Mahoney (San Francisco: ASP), p. 100

Shlosman, I., Frank, J., & Begelman, M. C. 1989, Nat, 338, 45

Sofue, Y., & Rubin, V. 2001, ARA&A, 39, in press (astro-ph/0010594)

Strickland, D. K., Heckman, T. M., Weaver, K. A., & Dahlem, M. 2000, AJ, 120, 2965

Surma, P., & Bender, R. 1995, A&A, 298, 405

Tran, H. D., Tsvetanov, Z., Ford, H. C., Davies, J., Jaffe, W., van den Bosch, F. C., & Rest, A. 2001, AJ, 121, 2928

van der Marel, R. P. 1999, AJ, 117, 744

van der Marel, R. P. 2001, in IAU Symp. 205, Galaxies and Their Constituents at the Highest Angular Resolutions, ed. R. Schilizzi, S. Vogel, E. Paresce, & M. Elvis (San Francisco: ASP), in press (astro-ph/0101166)

Wall, W. F., Jaffe, D. T., Bash, F. N., Israel, F. P., Maloney, P. R., & Baas, F. 1993, ApJ, 414, 98

Watson, W. D. 2001, in IAU Symp. 206, Cosmic Masers, ed. V. Migenes & E. Luedke (San Francisco: ASP), in press (astro-ph/0107572)

Wong, T., & Blitz, L. 2000, ApJ, 540, 771

Yates, J. A., Richards, A. M. S., Wright, M. M., Collett, J. L., Gray, M. D., Field, D., & Cohen, R. J. 2000, MNRAS, 317, 28

Discussion

Beckman: Did you make any attempt to take out the projected non-circular velocities when averaging your 2D velocity fields to yield the rotation curves in Hα for your galaxy centers?

Knapen: We have not yet explicitly attempted this but are very aware of the possible implications of this; e.g., when using the rotation curves to estimate the residual, or non-circular, motions (see Knapen et al. 2000a).

Erwin: In M100, am I correct in remembering that your model has both bars rotating at the same pattern speed?

Knapen: Yes, the model has both bars rotating at the same pattern speed, and the kinematics support this. In fact, we interpret M100 as a one-bar galaxy, where we see this one bar system bisected by the much more circular circumstellar ring.

Sheth: In the nuclear region, dust extinction can be extremely high and patchy, and your Hα FP velocity fields seem to be unaffected by dust extinction. Do the Hα velocity fields match those derived from CO emission or stellar kinematics?

Knapen: In those cases where comparable Hα and CO data are available, perhaps surprisingly, yes. CO usually follows the dust lanes, and although dust extinction generally follows a spiral pattern, Hα is offset from the dust and maybe that is why Hα velocity fields *work* in practice.

Kenney: How different would the observed velocity field in M100 be if the pattern speed of the inner bar were much higher? Would you detect such a difference?

Knapen: The velocity field itself does not give direct information on the inner bar pattern speed; we get this from a comprehensive comparison of numerical modeling with morphological and kinematic observations